Image Quality Measures and Their Performance

Ahmet M. Eskicioglu and Paul S. Fisher

Abstract— **A number of quality measures are evaluated for gray scale image compression. They are all bivariate, exploiting the differences between corresponding pixels in the original and degraded images. It is shown that although some numerical measures correlate well with the observers' response for a given compression technique, they are not reliable for an evaluation across different techniques. A graphical measure called Hosaka plots, however, can be used to appropriately specify not only the amount, but also the type of degradation in reconstructed images.**

I. Introduction

THE need for storing and transmitting huge volumes of data in today's computer and communications systems necessitates data compression in many fields ranging from medicine to aerospace. Data compression is an encoding process to reduce the storage and transmission requirements in applications. Many efficient techniques with considerably different features have recently been developed for both lossless and lossy compression. The evaluation of lossless techniques is normally a simple and straightforward task, where a number of standard criteria (compression ratio, execution time, etc.) are employed. A major problem in evaluating lossy techniques is the extreme difficulty in describing the type and amount of degradation in reconstructed images. Because of the inherent drawbacks associated with the subjective measures of image quality, there has been a great deal of interest in developing a quantitative measure, either in numerical or graphical form, that can consistently be used as a substitute. We would like to have such a measure not only to judge the quality of images obtained by a particular algorithm, but also for quality judgment across various algorithms. The latter task is definitely more challenging since a wide range of image impairments is involved. An extensive survey and a classification of the quality measures that appeared in the relevant literature are given in [1].

It is known that the mean square error (MSE), the most common objective criterion, or its variants do not correlate well with subjective quality measures. A major emphasis in recent research has therefore been given to a deeper analysis of the human visual system (HVS). The HVS is too complex to fully understand with present psychophysical means, but the incorporation of even a simplified model into objective measures reportedly leads to a better correlation with the response of the human observers.

Paper approved by M. R. Civanlar, the Editor for Image Processing of the IEEE Communications Society. Manuscript received February 22, 1994; revised August 1, 1994. This paper was presented in part at the 1994 Space and Earth Science Data Compression Workshop, Salt Lake City, UT, April 2, 1994.

The authors are with the Department of Computer Sciences, University of North Texas, Denton, TX 76203 USA.

IEEE Log Number 9415928.

TABLE I
IMAGE QUALITY MEASURES

Average Difference	$AD = \frac{1}{MN}\sum_{j=1}^{M}\sum_{k=1}^{N}[F(j,k)-\hat{F}(j,k)]$
Structural Content	$SC = \sum_{j=1}^{M}\sum_{k=1}^{N}[F(j,k)]^2 / \sum_{j=1}^{M}\sum_{k=1}^{N}[\hat{F}(j,k)]^2$
N. Cross-Correlation	$NK = \sum_{j=1}^{M}\sum_{k=1}^{N}F(j,k)\hat{F}(j,k) / \sum_{j=1}^{M}\sum_{k=1}^{N}[F(j,k)]^2$
Correlation Quality	$CQ = \sum_{j=1}^{M}\sum_{k=1}^{N}F(j,k)\hat{F}(j,k) / \sum_{j=1}^{M}\sum_{k=1}^{N}F(j,k)$
Maximum Difference	$MD = \mathrm{Max}\{\lvert F(j,k)-\hat{F}(j,k)\rvert\}$
Image Fidelity	$IF = 1-(\sum_{j=1}^{M}\sum_{k=1}^{N}[F(j,k)-\hat{F}(j,k)]^2 / \sum_{j=1}^{M}\sum_{k=1}^{N}[F(j,k)]^2)$
Weighted Distance	WD: Every element of the difference matrix is normalized in some way and L_1-norm is applied [1].
Laplacian Mean Square Error	$LMSE = \sum_{j=1}^{M-1}\sum_{k=2}^{N-1}[O\{F(j,k)\}-O\{\hat{F}(j,k)\}]^2 / \sum_{j=1}^{M-1}\sum_{k=2}^{N-1}[O\{F(j,k)\}]^2$
Peak Mean Square Error	$PMSE = \frac{1}{MN}\sum_{j=1}^{M}\sum_{k=1}^{N}[F(j,k)-\hat{F}(j,k)]^2 / [\mathrm{Max}\{F(j,k)\}]^2$
N. Absolute Error	$NAE = \sum_{j=1}^{M}\sum_{k=1}^{N}\lvert O\{F(j,k)\}-O\{\hat{F}(j,k)\}\rvert / \sum_{j=1}^{M}\sum_{k=1}^{N}\lvert O\{F(j,k)\}\rvert$
N. Mean Square Error	$NMSE = \sum_{j=1}^{M}\sum_{k=1}^{N}[O\{F(j,k)\}-O\{\hat{F}(j,k)\}]^2 / \sum_{j=1}^{M}\sum_{k=1}^{N}[O\{F(j,k)\}]^2$
L_p-norm	$L_p = \{\frac{1}{MN}\sum_{j=1}^{M}\sum_{k=1}^{N}\lvert F(j,k)-\hat{F}(j,k)\rvert^p\}^{1/p}, p = 1,2,3$
Hosaka plot	A graphical quality measure. The area and shape of the plot gives information about the type and amount of degradation [1,6].
Histogram	Another graphical quality measure. Gives the probability distribution of the pixel values in the difference image.

Note: For LMSE, $O\{F(j,k)\}=F(j+1,k)+F(j-1,k)+F(j,k+1)+F(j,k-1)-4F(j,k)$. For NAE, NMSE, and L_2-norm, $O\{F(j,k)\}$ is defined in three ways: (1) $O\{F(j,k)\}=F(j,k)$, (2) $O\{F(j,k)\}=F(j,k)^{1/3}$, (3) $O\{F(u,v)\}=H\{(u^2+v^2)^{1/2}\}F(u,v)$ (in cosine transform domain).

TABLE II
IMAGE COMPRESSION TECHNIQUES

JPEG	Fourth public release of the Independent JPEG Group's JPEG software
EPIC	Vision Science Group, The Media Laboratory, MIT
RLPQ	Department of Computer Sciences, University of North Texas
SLPQ	Department of Computer Sciences, University of North Texas

We attempt to evaluate the usefulness of some of the objective quality measures listed in [1] through a set of experiments.

II. Image Quality Measures, Compression Techniques, and Test Images

The quality measures included in our evaluation are listed in Table I. They are all discrete and bivariate, i.e., they provide some measure of closeness between two digital images by exploiting the differences in the statistical distributions of pixel values. $F(j,k)$ and $\hat{F}(j,k)$ denote the samples of original and degraded image fields.

TABLE III
TEST IMAGES

Image	Source	Size(bytesxbytes)	Pixel Length(bits)	Spatial Frequency
Lenna	NITF	512x512	8	14.07
Gilbert	US Navy	512x512	8	31.25
Fingerprint	NITF	512x512	8	59.37

TABLE IV-A
CORRELATION COEFFICIENTS FOR EACH TECHNIQUE (1) TEST IMAGE: LENNA (2) TEST IMAGE: GILBERT (3) TEST IMAGE: FINGERPRINT

Measure/Code	JPEG	EPIC	RLPQ	SLPQ
AD	0.528	-0.154	0.864	0.984
SC	0.561	-0.117	-0.988	-0.971
NK	0.479	0.865	0.996	0.979
CQ	0.480	0.865	0.996	0.979
LMSE	-0.980	-0.794	-0.752	-0.803
MD	-0.964	-0.984	-0.883	-0.941
WD	-0.995	-0.993	-0.954	-0.970
PMSE	-0.999	-0.996	-0.991	-0.990
IF	0.999	0.996	0.991	0.990
NAE	-0.997	-0.996	-0.970	-0.973
NAE(1/3)	-0.996	-0.996	-0.969	-0.972
NAE(HVS)	-0.972	-0.977	-0.925	-0.940
NMSE	-0.999	-0.996	-0.991	-0.990
NMSE(1/3)	-0.999	-0.997	-0.989	-0.989
NMSE(HVS)	-1.000	-0.998	-0.995	-0.996
L1	-0.997	-0.996	-0.970	-0.973
L2	-0.994	-0.993	-0.966	-0.969
L2(1/3)	-0.995	-0.993	-0.965	-0.968
L2(HVS)	-0.988	-0.990	-0.969	-0.975
L3	-0.991	-0.991	-0.961	-0.964

(1)

Measure/Code	JPEG	EPIC	RLPQ	SLPQ
AD	0.747	-0.527	0.820	0.969
SC	-0.243	-0.936	-0.987	-0.930
NK	0.768	0.981	0.984	0.936
CQ	0.768	0.981	0.984	0.936
LMSE	-0.869	-0.800	-0.809	-0.727
MD	-0.828	-0.929	-0.853	-0.687
WD	-0.960	-0.960	-0.958	-0.923
PMSE	-0.979	-0.986	-0.981	-0.943
IF	0.979	0.986	0.981	0.943
NAE	-0.967	-0.975	-0.975	-0.939
NAE(1/3)	-0.842	-0.987	-0.974	-0.945
NAE(HVS)	-0.941	-0.941	-0.961	-0.914
NMSE	-0.979	-0.986	-0.981	-0.943
NMSE(1/3)	-0.717	-0.992	-0.978	-0.958
NMSE(HVS)	-0.988	-0.989	-0.998	-0.967
L1	-0.967	-0.975	-0.975	-0.939
L2	-0.961	-0.965	-0.962	-0.917
L2(1/3)	-0.754	-0.985	-0.959	-0.934
L2(HVS)	-0.964	-0.968	-0.985	-0.941
L3	-0.948	-0.960	-0.946	-0.890

(2)

Measure/Code	JPEG	EPIC	RLPQ	SLPQ
AD	0.803	-0.101	0.926	0.880
SC	0.325	-0.846	-0.955	-0.935
NK	0.895	0.975	0.958	0.944
CQ	0.895	0.975	0.958	0.944
LMSE	-0.906	-0.962	-0.737	-0.812
MD	-0.417	-0.956	-0.540	-0.402
WD	-0.962	-0.992	-0.938	-0.934
PMSE	-0.989	-0.999	-0.962	-0.953
IF	0.989	0.999	0.962	0.953
NAE	-0.975	-0.994	-0.956	-0.946
NAE(1/3)	-0.974	-0.993	-0.954	-0.939
NAE(HVS)	-0.948	-0.987	-0.936	-0.925
NMSE	-0.989	-0.999	-0.962	-0.953
NMSE(1/3)	-0.988	-0.995	-0.959	-0.934
NMSE(HVS)	-0.991	-0.996	-0.966	-0.954
L1	-0.975	-0.994	-0.956	-0.946
L2	-0.975	-0.995	-0.947	-0.937
L2(1/3)	-0.974	-0.993	-0.943	-0.920
L2(HVS)	-0.968	-0.997	-0.946	-0.930
L3	-0.975	-0.996	-0.934	-0.925

(3)

Among the few models of the HVS that have been developed, we chose the one proposed by Nill for dealing with cosine transforms. The function for the model is defined as [2]

$$H(r) = \begin{cases} 0.05e^{r^{0.554}}, & \text{for } r < 7 \\ e^{-9[|\log_{10} r - \log_{10} 9|]^{2.3}}, & \text{for } r \geq 7, \end{cases}$$

TABLE IV-B
CORRELATION COEFFICIENTS ACROSS TECHNIQUES (1) TEST IMAGE: LENNA (2) TEST IMAGE: GILBERT (3) TEST IMAGE: FINGERPRINT

Measure/Ratio	69:1	59:1	52:1	42:1	30:1	20:1	10:1
AD	-0.470	-0.498	-0.051	-0.558	0.875	0.260	-0.656
SC	0.863	0.716	0.863	0.626	0.683	-0.780	0.364
NK	-0.834	-0.705	-0.834	-0.675	-0.582	0.858	-0.455
CQ	-0.834	-0.705	-0.834	-0.675	-0.582	0.858	-0.455
LMSE	0.231	0.163	-0.010	0.203	-0.720	-0.471	0.950
MD	0.033	0.564	0.332	0.541	-0.380	-0.958	0.681
WD	-0.914	-0.221	-0.097	0.519	-0.254	-0.792	0.941
PMSE	0.188	0.533	0.360	0.671	-0.085	-0.893	0.929
IF	-0.161	-0.520	-0.349	-0.666	0.087	0.892	-0.928
NAE	-0.805	-0.295	-0.133	0.534	-0.015	-0.862	0.915
NAE(1/3)	-0.790	-0.417	-0.302	0.434	-0.017	-0.858	0.915
NAE(HVS)	0.454	0.527	0.270	0.531	-0.272	-0.828	0.874
NMSE	0.161	0.520	0.349	0.666	-0.087	-0.892	0.928
NMSE(1/3)	-0.627	-0.342	-0.349	0.384	-0.119	-0.879	0.928
NMSE(HVS)	0.589	0.664	0.397	0.629	-0.202	-0.879	0.909
L1	-0.805	-0.295	-0.133	0.534	-0.015	-0.862	0.915
L2	0.164	0.503	0.332	0.651	-0.086	-0.884	0.932
L2(1/3)	-0.607	-0.313	-0.326	0.370	-0.123	-0.867	0.934
L2(HVS)	0.553	0.632	0.373	0.604	-0.187	-0.864	0.894
L3	0.461	0.627	0.401	0.670	-0.139	-0.893	0.938

(1)

Measure/Ratio	69:1	59:1	52:1	42:1	30:1	20:1	10:1
AD	-0.015	0.968	0.664	0.913	0.835	0.896	0.661
SC	-0.883	0.466	-0.494	-0.641	-0.552	-0.697	-0.739
NK	0.871	-0.654	0.617	0.728	0.636	0.760	0.741
CQ	0.871	-0.654	0.617	0.728	0.636	0.760	0.741
LMSE	0.532	-0.600	0.171	-0.112	-0.403	0.125	0.673
MD	-0.762	0.881	-0.935	-0.891	-0.761	-0.255	0.458
WD	-0.048	0.871	0.132	-0.365	-0.480	-0.639	-0.616
PMSE	-0.517	0.953	-0.700	-0.688	-0.788	-0.866	-0.753
IF	0.517	-0.953	0.700	0.688	0.788	0.866	0.753
NAE	-0.140	0.947	-0.011	-0.318	-0.374	-0.628	-0.759
NAE(1/3)	0.772	0.990	0.952	0.087	0.977	-0.174	-0.007
NAE(HVS)	-0.941	-0.961	-0.962	-0.896	-0.834	-0.854	-0.835
NMSE	-0.517	0.953	-0.700	-0.688	-0.788	-0.866	-0.753
NMSE(1/3)	0.560	0.993	0.961	0.118	0.982	-0.076	0.071
NMSE(HVS)	-0.967	-0.952	-0.973	-0.908	-0.843	-0.885	-0.895
L1	-0.140	0.947	-0.011	-0.318	-0.373	-0.628	-0.759
L2	-0.539	0.954	-0.712	-0.693	-0.786	-0.868	-0.754
L2(1/3)	0.584	0.999	0.935	0.084	0.974	-0.110	0.057
L2(HVS)	-0.965	-0.950	-0.967	-0.896	-0.832	-0.878	-0.881
L3	-0.787	0.984	-0.918	-0.904	-0.941	-0.893	-0.391

(2)

Measure/Ratio	69:1	59:1	52:1	42:1	30:1	20:1	10:1
AD	-0.871	0.878	-0.930	0.135	0.345	-0.093	-0.656
SC	-0.946	-0.925	-0.975	-0.960	-0.903	-0.953	-0.887
NK	0.979	0.930	0.982	0.971	0.924	0.966	0.920
CQ	0.979	0.930	0.982	0.971	0.924	0.966	0.920
LMSE	0.804	-0.437	-0.592	0.208	0.014	0.002	0.232
MD	0.735	0.977	0.999	0.309	0.573	-0.412	0.574
WD	0.057	-0.126	-0.976	-0.881	-0.918	-0.993	-0.930
PMSE	-0.185	0.916	-0.920	-0.983	-0.981	-0.989	-0.966
IF	0.185	-0.916	0.920	0.983	0.981	0.989	0.966
NAE	-0.304	1.000	-0.970	-0.999	-0.992	-0.989	-0.964
NAE(1/3)	-0.553	-0.024	-0.913	-0.994	-0.982	-0.980	-0.974
NAE(HVS)	-0.888	-0.404	-0.959	-0.977	-0.986	-0.946	-0.866
NMSE	-0.185	0.916	-0.920	-0.983	-0.981	-0.989	-0.966
NMSE(1/3)	-0.826	-0.791	-0.923	-0.986	-0.969	-0.976	-0.968
NMSE(HVS)	-0.894	-0.442	-0.986	-0.983	-0.979	-0.961	-0.902
L1	-0.304	1.000	-0.970	-0.999	-0.992	-0.989	-0.964
L2	-0.192	0.914	-0.921	-0.984	-0.983	-0.990	-0.964
L2(1/3)	-0.830	-0.792	-0.926	-0.987	-0.972	-0.974	-0.967
L2(HVS)	-0.896	-0.440	-0.988	-0.985	-0.983	-0.962	-0.892
L3	-0.195	0.862	-0.544	-0.960	-0.960	-0.988	-0.974

(3)

where $r = (u^2 + v^2)^{1/2}$, and u, v are the coordinates in the transform domain. The subimage structure weighting factor W_i in the original model was not used in our computations because we wanted to investigate the effect of $H(r)$ alone. Since W_i is proportional to the intensity level variance of subimage i, a separate analysis is needed to determine a suitable proportionality constant.

The implementations of the image compression techniques are given in Table II. Both JPEG and EPIC belong to the class of transform coding techniques. The former performs the discrete cosine transform and the latter a wavelet transform. RLPQ and SLPQ [3] contain several modifications to the Laplacian pyramidal decomposition and use a loose wavelet basis. After quantization, they employ arithmetic coding with

Fig. 1. Lena and four degraded versions: (a) Original; (b) JPEG; (c) EPIC; (d) RLPQ; (e) SLPQ.

a specifically tuned adaptive predictive model to compress the pyramid.

It should be noted that the choice of the compression techniques for an investigation of the performance of quality measures (especially those that are graphical) is important since it is desirable to include techniques which produce different types of impairments in the reconstructed images. Our purpose is to see how well the measures are able to describe image distortions of dissimilar nature. As we shall discuss later, the four codes in Table II serve this purpose.

The information about the three test images that we used can be seen in Table III. Lena and Fingerprint are in the set of the National Imagery Format Test Images. The third image, hurricane Gilbert, was obtained from the U.S. Navy.

The spatial frequency for a given image is defined as follows [4]:

Consider an $M \times N$ image, where M = number of rows and N = number of columns. The row and column frequencies are given by

$$\text{Row\_Freq} = \sqrt{\frac{1}{MN}\sum_{j=0}^{M-1}\sum_{k=1}^{N-1}[F(j,k) - F(j,k-1)]^2}$$

and

$$\text{Column\_Freq} = \sqrt{\frac{1}{MN}\sum_{k=0}^{N-1}\sum_{j=1}^{M-1}[F(j,k) - F(j-1,k)]^2}.$$

The total frequency is then

$$\text{Spatial frequency} = \sqrt{(\text{Row\_Freq})^2 + (\text{Column\_Freq})^2}.$$

This definition of frequency in the spatial domain indicates the overall activity level in an image.

(e)

Fig. 1. (continued)

III. Performance of Quality Measures

The gray scale image data set was obtained by coding and decoding the three test images with the compression codes listed in Table II. For each test image, seven different compression ratios were selected for degradation. They range from 10:1 to 70:1 with an increment of about 10. (Our original intention was to use the ratios 10:1, 20:1, 30:1, 40:1, 50:1, 60:1, and 70:1, but because of the inflexibility in using the JPEG parameter, we ended up with some different ratios.)

The photographic samples of the degraded images were first subjectively evaluated in an office environment by ten observers who were chosen from the graduate students and faculty having some background in image compression. They were asked to rank the images in two ways: Within each technique and between the four techniques for a fixed compression ratio. The mean rating of the group for an evaluation was computed by

$$R = \left(\sum_{k=1}^{10} s_k n_k\right) \Big/ \left(\sum_{k=1}^{10} n_k\right),$$

where s_k = the score corresponding to the kth rating, n_k = the number of observers with this rating, and 10 = the number of grades in the scale. The photographs were viewed at a distance at which 40 pixels subtended one degree of vision.

A. Numerical Measures

Table IV shows the correlation between the numerical objective quality measures and the subjective evaluation. As a measure of the extent of the linear relationship, the Pearson product-moment correlation coefficient (r) [5] was used. The possible values of r are between -1 and $+1$; the closer r is to -1 or $+1$, the better the correlation is.

The coefficient values in part (A) of Table IV indicate that the quality measures can be put into three groups according to their performance:

Group I: AD, SC
Group II: NK, CQ, LMSE, MD
Group III: WD, PMSE, IF, NAE, NMSE, L_p.

The measures in Group I cannot be reliably used with all techniques as the sign of the correlation coefficient does not remain the same. Group II measures are consistent, but nevertheless have poor correlation with the observers' response for some of the techniques. Among the useful measures in Group III, NMSE(HVS) is the best one for all the test images. Except for a single case, the incorporation of the HVS into NMSE makes the correlation slightly stronger. For the other two measures NAE and L_2, however, there is no such improvement. (In fact, the visual model has an adverse effect on NAE.) The results reported in [6] and [7] support our conclusion that the HVS model does not always improve the correlation, and when it does, the gain is small. The nonlinear filter $(\bullet)^{1/3}$, on the other hand, seems to have a random behavior, but usually leads to a weaker correlation. As PNMSE and IF are defined in terms of NMSE, they establish the same relationship.

Part (B) of Table IV is rather disappointing, and the information that can be extracted is limited. As the compression ratio is increased, the performance of the measures becomes much poorer. This observation is not surprising because different techniques introduce different types of degradation into the reconstructed images. Since the metrics combine all the pixel differences between two given images into a single number, one cannot expect to know much about the annoyance experienced by the human observer. In our experiments, for instance, the observers found the tile effect very objectionable in Lena, yet favored blockiness in the higher frequency images Gilbert and Fingerprint.

An important observation made in applying the Group III numerical measures to images is that the higher the original image frequency the larger the error for a given compression technique and a given compression ratio. A representative

TABLE V
A SUBSET OF NMSE (HVS) VALUES

	Compression ratio = 69:1			Compression ratio = 10:1		
Code\Image	Lenna	Gilbert	Fingerprint	Lenna	Gilbert	Fingerprint
JPEG	0.159	0.341	0.541	0.012	0.061	0.106
EPIC	0.289	0.558	0.730	0.017	0.115	0.170
RLPQ	0.434	0.629	0.746	0.039	0.120	0.168
SLPQ	0.380	0.580	0.712	0.044	0.135	0.192

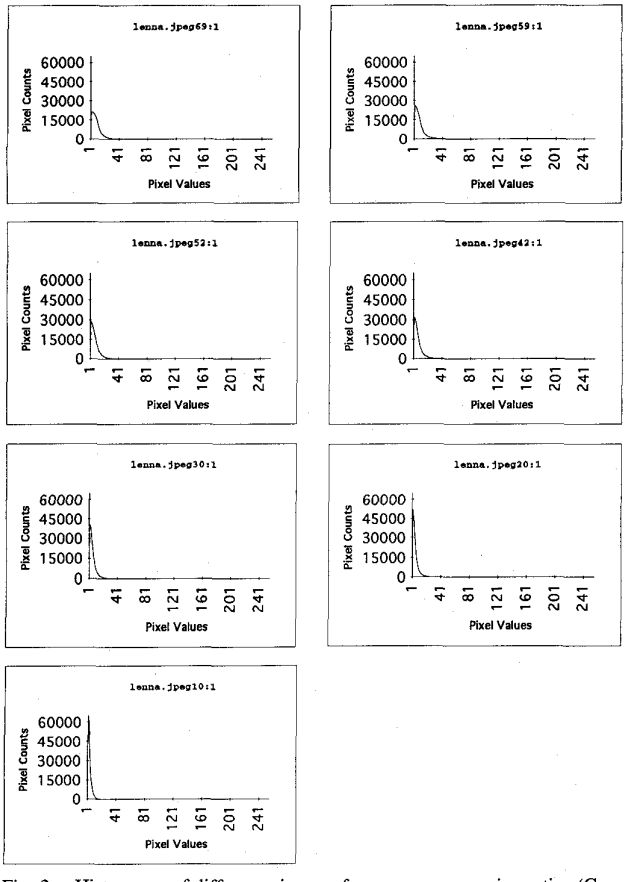

Fig. 2. Histograms of difference images for seven compression ratios (Compression technique = JPEG).

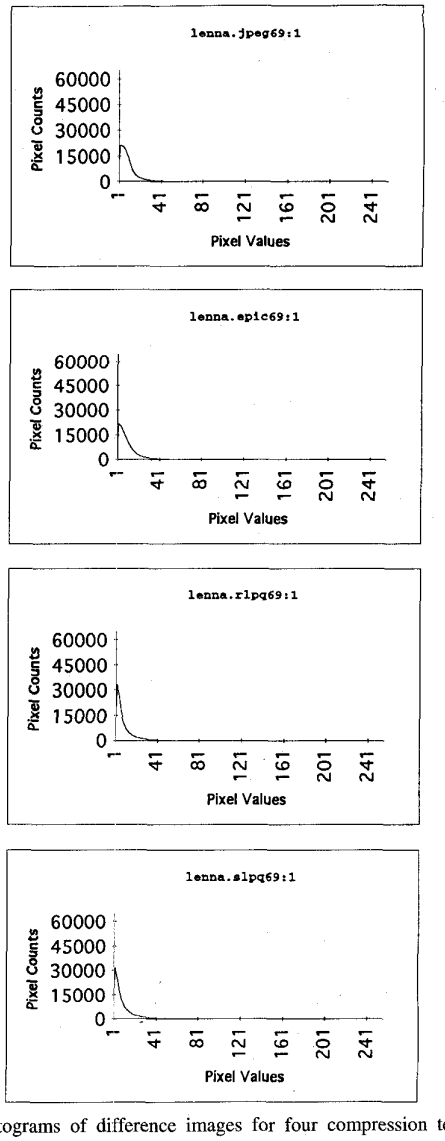

Fig. 3. Histograms of difference images for four compression techniques (Compression ratio = 69:1).

subset in Table V shows that the smallest NMSE(HVS) values are associated with Lena, and the largest with Fingerprint. There is one thing worth mentioning at this point. If the image variance was used as an indicator of the activity level, we would not have such a relationship because the biggest variance belongs to Gilbert (The variances are 2299 for Lena, 5012 for Gilbert, and 3839 for Fingerprint).

B. Graphical Measures

To the best of our knowledge, histograms and Hosaka plots are the only two image quality measures that are graphical. Before we evaluate their performance, a specification of the type of impairment caused by the techniques is needed. Because of space limitation, the results for only the first test image will be discussed here. Four degraded versions of Lena for the highest compression ratio (69:1) are given in Fig. 1. The original image is also included for a comparison. The major types of degradation in the images are blockiness with JPEG, blurriness with EPIC, both fuzziness and blockiness with RLPQ, and fuzziness with SLPQ (The term fuzziness is used in the sense of equal amount of blurriness over the entire image).

A histogram of the compression error is constructed by plotting the number of times a specific value occurs in the difference image versus the value itself. Typically, it looks like a Gaussian curve; the more it resembles a spike at $x = 0$, the greater the fidelity of the reconstructed image. Because of the symmetric characteristic of the distribution, an alternative would be to use the absolute values of the pixels. The seven histograms in Fig. 2 were obtained using this approach. They clearly depict the increase in the amount of blockiness as the compression ratio goes up. The concentration of low intensity pixels for the lowest ratio is gradually reduced and the distribution becomes more uniform. Our experience has shown that histograms cannot be used to specify different types of degradation in images. In Fig. 3, the histograms with low intensity pixel concentrations are associated with RLPQ

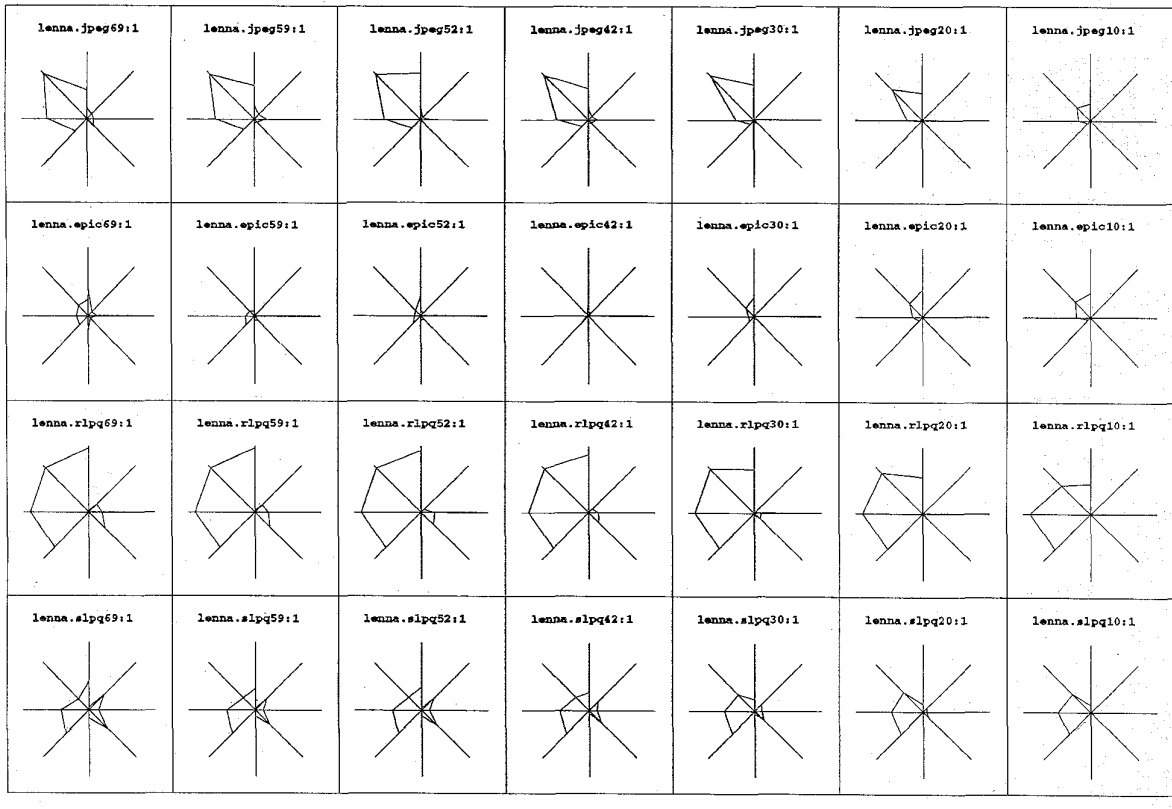

Fig. 4. Hosaka plots.

and SLPQ, and they are in contrast with those corresponding to JPEG and EPIC. Causing a global loss of sharp details, fuzziness results in smaller image variances, which, in turn, lead to spiky histograms. Nevertheless, the similarity between the histograms in each pair makes it difficult to distinguish between the artifacts involved.

To construct a Hosaka plot, or an h-plot, we measure a pair of features of the reconstructed image and compare these with the corresponding features in the original image [8], [9]. The difference between the two feature vectors generates a vector error measure, which, unlike scalar quantities, allows for a description of not only the amount, but also the type of degradation. In the process, the original image is first segmented into blocks whose variance is less than some specified threshold. These blocks are then grouped together to form a number of classes which depend on the size of the blocks. Two features are computed for each class in both the original and the reconstructed images. One of them is related to the mean intensity values and the other is the mean standard deviation. The h-plot is constructed by plotting the errors in the corresponding features in polar coordinates. The radius denotes the feature error, the left and right half planes contain the vectors associated with standard deviations and means, respectively.

Three controlled examples are presented in [9] to illustrate the use of h-plots. The first consists of adding a dc shift to the image, the second is the inclusion of noise, and the third is the blurring of the image. It is reported that the area of the h-plot is proportional to the image quality while the structure of the diagram depends on the type of distortion.

The h-plots in Fig. 4 were obtained using Lena for all compression techniques and ratios. In each diagram, the length of a radius is 2.75 units. The blockiness is reflected on the left side of h-plots, whereas, the effect of blurriness can be traced on the right. By a simple comparison, we are able to see the way each code reduces the fidelity of the image. One can even learn how the distortion is distributed in the reconstructed images by looking at the relative lengths of the components along the axes. For example, it is evident that JPEG preserves the high frequency components (the feathers) of the image, whereas RLPQ induces uniform blockiness. Such information is extremely helpful considering the sensitivity of the human observer to the location of the image error.

For the construction of the h-plots in Fig. 4, the two parameters, the initial block size N and the variance threshold T, were chosen as 16 and 10, respectively, as in Hosaka's or Farrelle's work [8], [9]. Our experimentation, however, showed that the selection of suitable values for these two parameters is not straightforward, and strongly depends on

1) the compression ratio,
2) the spatial frequency,
3) the type of impairment.

This dependence can be observed in Fig. 4. The h-plots for JPEG and RLPQ indicate that when a wide range of compression ratios is used, it may be worth trying larger values for T and N.

IV. Conclusion

The results of an evaluation concerning the usefulness of a number of objective quality measures for grayscale image compression have been presented. It is demonstrated that although a group of numerical measures can reliably be used to specify the magnitude of degradation in reconstructed images for a given compression technique, an evaluation across different techniques is not possible. This is because a single scalar value cannot be used to describe a variety of impairments. A simple analogy would be the futility in comparing apples with oranges. Hosaka plots, however, provide a good indication of how images are degraded, and they are particularly useful when the impairment is blockiness. A practical problem for their construction appears to be the proper selection of the two parameters, which may require some insight and experience.

We believe that a combination of numerical and graphical measures may prove more useful in judging image quality. There is also a need for the development of new graphical measures with superior judgment capabilities. One possible avenue of progress would be to use different features for Hosaka plots (e.g., higher order moments, symmetry measures or local spectrum). Further research in these areas is now ongoing.

Acknowledgment

The authors thank Mr. Siyuan Chen for his assistance in running the programs and preparing the histograms and Hosaka plots.

References

[1] A. M. Eskicioglu and P. S. Fisher, "A survey of quality measures for gray scale image compression," in *Proc. 1993 Space and Earth Science Data Compression Workshop* (NASA Conference Publication 3191), Snowbird, Utah, Apr. 2, 1993, pp. 49–61.

[2] N. B. Nill, "A visual model weighted cosine transform for image compression and quality assessment," *IEEE Trans. Commun.*, vol. COM-33, no. 6, pp. 551–557, June 1985.

[3] O. Kiselyov, "Multiresolutional/fractal compression of still and moving pictures," Ph.D. Dissertation, Department of Computer Sciences, University of North Texas, USA, Dec. 1993.

[4] P. S. Fisher and N. Tavakoli, Final Report for Compression of Geophysical Data, Space and Naval Warfare Systems Command Contract N00039-C-0063, Department of Computer Sciences, University of North Texas, May 1992.

[5] A. C. Bajpai, I. M. Calus and J. A. Fairley, *Statistical Methods for Engineers and Scientists.* New York: Wiley, 1979, p. 370.

[6] G. G. Kuperman and D. L. Wilson, "Objective and subjective assessment of image compression algorithms," in *Society for Information Display Int. Symp. Digest of Technical Papers*, vol. 22, pp. 627–630, 1991.

[7] J. Farrell, H. Trontelj, C. Rosenberg, and J. Wiseman, "Perceptual metrics for monochrome image compression," in *Society for Information Display Int. Symp. Digest of Technical Papers*, vol. 22, pp. 631–634, 1991.

[8] K. Hosaka, "A new picture quality evaluation method," in *Proc. Int. Picture Coding Symp.*, Tokyo, Japan, Apr. 1986, pp. 17–18.

[9] P. M. Farrelle, *Recursive Block Coding for Image Data Compression.* New York: Springer-Verlag, 1990.

Ahmet M. Eskicioglu received the B.S. degree in mathematics from the Middle East Technical University, Ankara, Turkey, and the M.S. and Ph.D. degrees in control engineering from the University of Manchester Institute of Science and Technology, Manchester, England.

He was on the faculty of the Computer Engineering Department at the Middle East Technical University from 1983 to 1992 before he came to the University of North Texas as a visiting professor. Dr. Eskicioglu is currently an adjunct professor at the same institution. His research interests include data and image compression, optimization, and system simulation.

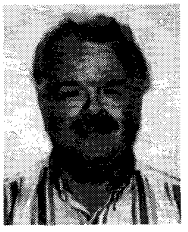

Paul S. Fisher was awarded degrees in mathematics (B.A.'63, M.A.'64) from the University of Utah, and a Ph.D. in computer science from Arizona State University in 1969.

He is presently a Professor in the Department of Computer Sciences at the University of North Texas, having served as its chair from 1989 to 1994. Prior to that he owned and operated his own company, Computer and Information Sciences, Inc. between 1982 and 1989. From 1967 until 1988 he was on the faculty at Kansas State University, Manhattan, KS, and served as chair of the Computer Science Department for eleven years. His present interests are in image and video compression, and pattern recognition including speech and signal processing.